

This discussion paper is/has been under review for the journal Atmospheric Chemistry and Physics (ACP). Please refer to the corresponding final paper in ACP if available.

# Simultaneous HONO measurements in and above a forest canopy: influence of turbulent exchange on mixing ratio differences

M. Sörgel<sup>1</sup>, I. Trebs<sup>2</sup>, A. Serafimovich<sup>3</sup>, A. Moravek<sup>2</sup>, A. Held<sup>1</sup>, and C. Zetzsch<sup>1,4</sup>

<sup>1</sup>University of Bayreuth, Atmospheric Chemistry Research Laboratory, 95440 Bayreuth, Germany

<sup>2</sup>Max Planck Institute for Chemistry, Biogeochemistry Department, P.O. Box 3060, 55020 Mainz, Germany

<sup>3</sup>University of Bayreuth, Department of Micrometeorology, 95440 Bayreuth, Germany

<sup>4</sup>Fraunhofer Institute for Toxicology and Experimental Medicine, 30625 Hannover, Germany

Received: 13 August 2010 – Accepted: 20 August 2010 – Published: 3 September 2010

Correspondence to: M. Sörgel (matthias.soergel@uni-bayreuth.de)

Published by Copernicus Publications on behalf of the European Geosciences Union.

21109

## Abstract

We have combined chemical and micrometeorological measurements to investigate the formation and distribution of HONO throughout a forest canopy. HONO was measured simultaneously at two heights, close to the forest floor and just above canopy. The turbulent exchange between the forest and the atmosphere above was studied using vertical profiles of eddy covariance measurements. HONO mixing ratios at both heights showed typical diel cycles with low daytime values (~80 ppt) and high nighttime values (up to 500 ppt), but were influenced by various sources and sinks leading to mixing ratio differences (above canopy minus below) of up to +240 ppt at nighttime. In the late afternoon and early night mixing ratios increased at higher rates near the forest floor, indicating a possible ground source. Due to the simultaneous decoupling of the forest from the air layer above the canopy, mixing ratio differences reached about –170 ppt. From the late night until the early morning mixing ratios above the forest were typically higher than close to the forest floor. For some cases, this could be attributed to advection above the forest, which only partly penetrated the canopy. Measured photolysis frequencies above and below the forest canopy differed by a factor of 10–25 resulting in HONO lifetimes of about 10 min above and 100–250 min below the canopy at noontime. However, these differences of the main daytime HONO sink were not evident in the mixing ratio differences, which were close to zero during the morning hours. Effective turbulent exchange due to a complete coupling of the forest to the air layer above the canopy in the morning has offset the differences caused by the daytime photolytic sink and added to the interplay between different HONO production and loss processes.

## 1 Introduction

Nitrous acid (HONO,  $\text{HNO}_2$ ) is currently gaining substantial attention due to its contribution to the tropospheric OH radical production, which is the “cleansing detergent”

21110





research site is located in the Fichtelgebirge mountains in Northeast Bavaria (50° 9' N, 11° 52' E, 775 m a.s.l.), Germany, in a rural forested region. This site has been extensively studied by the University of Bayreuth (Matzner, 2004) and is a part of the FLUXNET (Baldocchi et al., 2001). Detailed information about the site has been given by Gerstberger et al. (2004). The site is covered by a Norway spruce (*Picea abies* (L.) Karst.) forest with a canopy height of 23–25 m (Staudt and Foken, 2007). A detailed description of the aims of the EGER project and the instrumental setup employed during the IOPs has been given by Foken et al. (2010). The measurements discussed in this paper were made at three different sites in the forest stand. A thin 36 m high tower (“turbulence tower”) located about 60 m southeast of the main tower (31 m walk-up tower) was used for (undisturbed) turbulence measurements. The *forest floor exchange site* was located about 30 m northwest of the main tower.

Simultaneous measurements of HONO were conducted at a height of 24.5 m (just above canopy) on the main tower and close to the forest floor in 0.5 m at the *forest floor exchange site* from 13–25 September 2007. HONO was measured by two LOPAP instruments (LONG Path Absorption Photometer, QUMA Elektronik and Analytik, Wuppertal, Germany). The LOPAP is based on a wet chemical technique, with fast sampling of HONO as nitrite in a stripping coil and subsequent detection as an azo dye using long path absorption in 2.4 m long Teflon AF tubing. A detailed description of the instrument has been given by Heland et al. (2001) and Kleffmann et al. (2002). The instruments were placed outside in the forest or directly on the tower in ventilated aluminum boxes without temperature control. The temperature of the stripping coils was kept constant at 20 °C by thermostats to assure constant sampling conditions.

From 29 September to 3 October both LOPAPs were compared side-by-side near the forest floor at a height of 1 m. The sampling inlets had a distance of about 50 cm and were directed northwards to sample perpendicularly to the westerly flow. No T-piece was used as inlet to avoid artificial HONO formation or adsorption on the inner walls of the tubing. Both instruments were supplied with the same reagents via T-pieces.

21115

Temperature and humidity profiles were measured at the main tower using Frankenberger-type psychrometers (Frankenberger, 1951). The relative humidity (RH) was calculated from the dry and wet bulb temperature of the psychrometers using the Magnus formula after Sonntag (1990) for the saturation vapour pressure and the Sprung formula for the actual vapour pressure (Foken, 2008). Psychrometers were mounted on the main tower at 0, 2, 5, 12, 21 and 32 m. Additionally, visibility was measured with a PWD11 (Vaisala, Vantaa, Finland) present weather detector mounted on the main tower.

Aerosol number size distributions were measured on the main tower at 28 m height using a Scanning Mobility Particle Sizer (SMPS, Grimm, Ainring, Germany). Boundary layer heights were derived from SODAR (SOund Detection And Ranging, Metek Meteorologische Messtechnik, Elmshorn, Germany) measurements at a nearby clearing.

Vertical profiles of nitrogen oxides (NO and NO<sub>2</sub>) were measured on the main tower and on the *forest floor exchange site* by red-filtered detection of the chemiluminescence produced by the reaction of NO with O<sub>3</sub> (CLD 780 TR, ECO Physics, Duernten, Switzerland). NO<sub>2</sub> was photolytically converted to NO by exposure of the sample air to a solid-state blue-light converter (Meteorologie Consult, Königstein, Germany) and subsequently detected by the chemiluminescence analyzer. Sample air was drawn through 55 m of non-transparent and heated PFA tubing from each inlet height. Inlet heights of the system were located at 0.05, 0.3, 1, 2, 5, 10, 16, and 24 m. The lower heights of up to 2 m were located at the *forest floor exchange site*, while the upper heights were mounted at the main tower, for details see Moravek (2008).

To detect the coupling regimes between the subcanopy, canopy and layer above the canopy the eddy-covariance measurements were used. Six eddy-covariance systems consisting of a sonic anemometer and fast response CO<sub>2</sub> and H<sub>2</sub>O gas analyzers were installed at the turbulence tower in 2.25, 5.5, 13, 18, 23 and 36 m. The wavelet transform was used to detect and extract ramp-like structures (coherent structures) from high frequency measurements of wind, sound temperature, CO<sub>2</sub> and H<sub>2</sub>O concentrations (Thomas and Foken, 2005). These structures are responsible for the turbulent

21116

coherent transport of the momentum and matter in forested ecosystems. Analysis of a sensible heat transport by coherent structures reveals the portions of the forest canopy coupled by coherent exchange with the air above the canopy (Thomas and Foken, 2007). The experimental setup and the analysis of the coupling regimes during the EGER intensive observation periods are described in more detail by Serafimovich et al. (2010).

The HONO photolysis frequency ( $j(\text{HONO})$ ) was calculated from the  $\text{NO}_2$  photolysis frequency measured by filter radiometers (Meteorologie consult, Königstein, Germany) according to Kraus and Hofzumahaus (1998) and Trebs et al. (2009). The radiometers were mounted on top of the main tower at a height of 28 m, and at 2 m above the forest floor at the *forest floor exchange site*.

For statistical computing the free statistics software “R” was used (<http://www.R-project.org>).

### 3 Results and discussion

#### 3.1 Comparison of the two LOPAP instruments

The LOPAP instruments from the University of Bayreuth (UBAY) and the Max-Planck-Institute for Chemistry (MPIC) were compared side-by-side at 1 m above the forest floor between 27 September and 3 October to evaluate the precision of the instruments. For this purpose the relative differences of the measured HONO mixing ratios were calculated by normalizing the difference of  $[\text{HONO}]_{\text{UBAY}} - [\text{HONO}]_{\text{MPIC}}$  by the arithmetic mean of these mixing ratios. The temporal evolution of these relative mixing ratio differences is shown in Fig. 1 together with the visibility as an indicator of foggy events. During rainy and foggy weather conditions indicated by the reduced visibility, we observed systematic deviations between the two LOPAP instruments. Large relative differences of the HONO signals during periods with low visibilities are related to fog events. Bröske et al. (2003) reported no measurable particle losses in the sampling glass coil for SOA

21117

(secondary organic aerosol) particles with diameters from 50–800 nm but Kleffmann et al. (2006) argued that large particles like fog droplets might be sampled by the coil. Thus, the sampling of fog droplets containing nitrite is a plausible explanation for deviations under wet conditions. However, this should affect both instruments by introducing more scatter and cannot explain the systematic deviation. Another potential reason could be that the surfaces of the sampling coils exhibited different wettabilities during these periods. During the dry conditions (visibilities of more than 2000 m, which is the maximum detectable by the instrument) between 29 September (14:00 CET) and 2 October (10:00 CET) HONO levels ranged from 35 ppt to 170 ppt and the instruments agreed within 12% ( $2\sigma$ ), which is within the range of the estimated instrumental error under the given conditions (e.g., detection unit not air conditioned). Omitting the wet conditions before and after the dry period the relative errors correspond to a Gaussian distribution centred at zero. Thus, no systematic deviation of the instruments was found during dry conditions. The insert on Fig. 1 shows the correlation between the two instruments. Applying standard major axis regression analysis (Sokal and Rohlf, 1995; Legendre and Legendre, 1998), which is suitable for two random variables (e.g., Ayers, 2001) by reducing deviations perpendicularly to the regression line, yields an intercept of 2.3 ppt, which is close to the detection limit of the instruments ( $3\sigma$ -definition). The slope is 0.97 and the coefficient of determination  $r^2=0.98$  for the dry weather period. Kleffmann (2006) used a T-piece and PFA tubing in front of the sampling units to compare two LOPAP instruments in order to avoid any influence from inhomogeneities in the sampled air. The linear correlation of these two LOPAPs was very good over a large mixing ratio range from about 200 ppt to 1.6 ppb, with a slope of 0.993 and an intercept of 1.4 ppt. However, since it is well known that any tubing in front of the sampling unit may cause artefacts due to wall reactions of  $\text{NO}_2$  we avoided this approach. Furthermore, there was no dependency of the relative error on the friction velocity ( $U^*$ ) or the horizontal wind speed, indicating no significant influence from inhomogeneities in the sampled air. This is expected because the sampling units were only about 50 cm apart. At wind speeds as low as  $0.5 \text{ m s}^{-1}$  it took only 1 s to pass both sampling units,

21118

whereas the response time of both instruments is about 7 min. Thus, small scale inhomogeneities should contribute equally to both signals.

We conclude that the LOPAP instruments can be used to reliably measure vertical HONO mixing ratio differences under dry conditions.

## 5 3.2 Factors controlling HONO mixing ratio levels

### 3.2.1 General observations in the time series

HONO is effectively scavenged by precipitation due to its good water solubility with a Henry's law constant of about  $5 \text{ mol L}^{-1} \text{ atm}^{-1}$  (Sander, 1999). Precipitation was found to structure the time series ranging from 13 of September to 3 October on a time scale of about a week due to synoptic weather conditions (low and high pressure systems). Although not precisely measurable (see Sect. 3.1) due to large relative errors of both instruments during foggy conditions, HONO values were clearly lower at both heights during these wet periods. HONO/NO<sub>x</sub> ratios were below 2% at both heights because (due to lower Henry's law constants of NO (about  $2 \times 10^{-3} \text{ mol L}^{-1} \text{ atm}^{-1}$ ) and NO<sub>2</sub> ( $1\text{--}4 \times 10^{-2} \text{ mol L}^{-1} \text{ atm}^{-1}$ ) (Sander, 1999)) NO<sub>x</sub> is not significantly influenced by precipitation scavenging or enhanced deposition on wet surfaces. During the entire IOP, three dry periods occurred between rain events. Dry periods were characterized by steadily increasing nighttime HONO mixing ratios up to 500 ppt, while HONO mixing ratios dropped during rain events to about 20 ppt. One of these dry periods (20–25 September) is shown in Fig. 2. At the beginning of the dry period, HONO increased continuously with a rate of about  $2 \text{ ppt h}^{-1}$  without a pronounced diel cycle, although the 20 September was a clear-sky day with  $j(\text{HONO})$  values of about  $0.002 \text{ s}^{-1}$  around noon (see Fig. 3).

An increasing trend in both the time series of the HONO mixing ratio and the HONO/NO<sub>x</sub> ratio is evident. To our knowledge this type of accumulation behaviour was not reported so far, and it was not directly linked to an increase of the precursor NO<sub>2</sub>. Although clarifying the reason for this is far beyond our applied measurement

21119

setup, a mechanism that might explain these observations would be the accumulation of (photo-) chemically formed or deposited HONO at the surface and the subsequent release by increasing RH, according to a Langmuir-type surface mechanism proposed by Trick (2004) due to enhanced adsorption of water molecules and subsequent release of HONO, as RH increases in the late afternoon. Additionally, HONO formation due to photolysis of deposited HNO<sub>3</sub>/nitrate as suggested by Zhou et al. (2002a,b, 2003) might be an explanation, since the precursor ("sticky" HNO<sub>3</sub>) is deposited efficiently to the canopy (Wolff et al., 2010) and accumulates at the needle surface (Zhou et al., 2002a).

### 10 3.2.2 S/V<sub>ground</sub> versus S/V<sub>aerosol</sub>

The needle surface also constitutes the largest fraction of the total ground surface. Therefore, we estimated the ground surface from measurements of the projected plant surface neglecting stem and understory contributions. The average PAI (Plant Area Index) of this forest stand is  $5 \text{ m}^2 \text{ m}^{-2}$  (Staudt et al., 2010). This projected area can be converted to a surface area by multiplying with  $\pi$  for wooden parts (assuming they are round), which contribute about 20% (5–35%, Gower et al., 1999) to the PAI and by a factor of 2.65 derived by Oren et al. (1986) to convert the projected LAI (~80% of PAI) to the geometric needle surface. From that simple scheme we derive a total geometric surface of the crown of  $13.7 \text{ m}^2 \text{ m}^{-2}$  ( $10.6 \text{ m}^2 \text{ m}^{-2}$  needle surface and  $3.6 \text{ m}^2 \text{ m}^{-2}$  wooden surface). From SODAR (SOund Detection And Ranging) measurements we inferred an average NBL (Nocturnal Boundary Layer) height of 120 m by a steep change in reflectivity of the sound signal. Using this value as an upper limit for the volume ( $1 \text{ m}^2$  as base area), and for a lower limit ground surface the geometric needle surface of the canopy, we get a  $S/V_{\text{ground}}$  of  $0.1 \text{ m}^{-1}$ , which is an order of magnitude higher than e.g. reported by Yu et al. (2009). However, Yu et al. (2009) took only the inverse of the mixed layer height as  $S/V_{\text{ground}}$ , not accounting for any roughness of the surface. Especially, during nighttime the boundary layer height represents an upper limit for the volume, because mixing is very limited within the stable thermally stratified

21120

NBL (Stull, 1988). Vogel et al. (2003) used a value of  $0.1 \text{ m}^{-1}$  to model heterogeneous HONO production in the lowest box of their model but increased  $S/V_{\text{ground}}$  to  $0.3 \text{ m}^{-1}$ , which matched the observations better. This is consistent with our observations that ( $S/V_{\text{ground}}$ )  $0.1 \text{ m}^{-1}$  reflects a lower limit. In contrast, the  $S/V_{\text{ground}}$  values given by Lam-  
 5 mel and Cape (1996) were an order of magnitude higher, e.g., considering vegetation surfaces with  $0.6\text{--}1.4 \text{ m}^{-1}$  (for a mixed layer height of 100 m). Additionally, we calculated the aerosol surface from the measured aerosol number size distributions and we found that  $S/V_{\text{aerosol}}$  was typically less than 1% of  $S/V_{\text{ground}}$ , which implies that the contribution of aerosol surfaces to HONO formation can be neglected for our study.

10 A decrease of the boundary layer height increases  $S/V_{\text{ground}}$ . Hence, with the same surface more HONO is concentrated in a smaller volume. However, at the same time turbulence is suppressed during these stable conditions. This reduces the exchange between the atmosphere and the surface.

### 3.2.3 Nighttime HONO conversion frequencies

15 HONO nighttime conversion frequencies  $\bar{F}_{\text{HONO,night}}$  from the heterogeneous disproportionation of  $\text{NO}_2$  (cf. R1) can be estimated for the dry periods. Su et al. (2008) discussed the problem of different scaling methods for HONO production and suggested to use a combined scaling approach of different quantities emitted close to the ground like black carbon (HONO/BC) or carbon monoxide (HONO/CO), and the “classical” HONO/ $\text{NO}_2$  or HONO/ $\text{NO}_x$ . The scaling was (originally) introduced to reduce  
 20 influences from boundary layer processes such as dilution or vertical mixing. However, local sources of the scaling quantities will affect the ratio (Su et al., 2008). As discussed above, humid surfaces or precipitation will also alter the HONO/ $\text{NO}_x$  ratio due to different solubilities as well as the advection of  $\text{NO}_x$  from road traffic during the morning hours at our site. Due to the lack of carbon monoxide (CO) and black carbon  
 25 (BC) measurements we use the  $\text{NO}_x$  scaling approach, which was used in many other studies (e.g., Sjödin, 1988; Alicke et al., 2002; Kleffmann et al., 2003). The approach

21121

of Alicke et al. (2002) for inferring conversion frequencies, taking a linear increase of HONO during nighttime divided by the average  $\text{NO}_2$  mixing ratio in this time interval is most commonly used.

$$\bar{F}_{\text{HONO,night}} = \frac{[\text{HONO}](t_2) - [\text{HONO}](t_1)}{(t_2 - t_1)[\text{NO}_2]_{\text{night}}} \quad (1)$$

5 There is still no reliable way of inferring HONO conversion frequencies using objective criteria. Yu et al. (2009) used a fixed time interval from 18:00 LT to midnight (local time) to determine HONO conversion frequencies. This approach leads to a very large scatter in our conversion frequencies. In addition, it yields mainly negative conversion frequencies in the lower height, because HONO increases already before sunset, thus  
 10 starting at higher levels, and peak mixing ratios are reached before midnight. We also tried an approach different from the “classical” one, not using the maximum HONO mixing ratio as end point but the maximum HONO/ $\text{NO}_x$  ratio that can be regarded as the maximum amount of HONO produced by  $\text{NO}_x$ .

1) Evaluating individual increases of HONO by the “classical” approach, excluding ad-  
 15 vection events and other disturbances

This approach could be used for evaluating data from five nights of the whole IOP (13–  
 20 25 September) and yielded a value of  $\bar{F}_{\text{HONO,night}} \pm \sigma = (1.1 \pm 0.65) \% \text{ h}^{-1}$  for the measurements above the canopy and a value of  $(0.75 \pm 0.45) \% \text{ h}^{-1}$  close to the ground. The lower value for the lower height may be caused by choosing the starting point after sunset, whereas the first pronounced increase in HONO mixing ratios occurs already in the hours before sunset. Thus, the starting mixing ratio level is already higher at the lower height, whereas the increase at the upper height normally occurs later and is therefore completely captured. However, the influence of photochemistry has to be excluded for a proper comparison of heterogeneous production, and therefore we cannot  
 25 use the data before sunset. The values of  $\bar{F}_{\text{HONO,night}}$  at both heights agree within their standard deviation (variation over five nights) and are consistent with literature values

21122

between  $0.4\% \text{ h}^{-1}$  and  $1.8\% \text{ h}^{-1}$  recently summarized by Su et al. (2008). The value for the upper height also compares quite well with a value of  $1.4 \pm 0.4\% \text{ h}^{-1}$  reported by Yu et al. (2009), which was not included in the comparison by Su et al. (2008).

2) Evaluating the period from sunset to the maximum HONO/NO<sub>x</sub> ratio

5 Conversion frequencies inferred by this approach are identical to the “classical” ones for the conditions during our campaign. The values and the variation of HONO/NO<sub>x</sub> ratios were mainly correlated to HONO mixing ratios (see Fig. 4a,b). Therefore, the HONO/NO<sub>x</sub> maxima occurred simultaneously with the maximum HONO mixing ratios (Fig. 2). Additionally, HONO mixing ratios were nearly independent of its precursor  
 10 NO<sub>2</sub> (see Fig. 4c). This was attributed to the fact that in contrast to studies in urban areas low NO<sub>2</sub> mixing ratios were prevailing. About 90% of the NO<sub>2</sub> values were below 5 ppb and 70% of the values ranged between 1 and 4 ppb, indicating quite constant NO<sub>2</sub> levels. The highest HONO and HONO/NO<sub>x</sub> values typically occurred before or around midnight (see Fig. 2) at moderate (2–5 ppb) NO<sub>2</sub> mixing ratios, whereas the  
 15 highest NO<sub>x</sub> values occurred in the morning hours (advection from road traffic). The weak correlation of HONO to NO<sub>x</sub> has already been observed in a field study at a rural forested site (Zhou et al. 2002a).

Nevertheless, conversion frequencies, as summarized above, are within the range of values reported in literature. Referring to the different conditions and methods used in  
 20 these experiments, this range is astonishing narrow and might provide some guidance for modelling studies.

### 3.3 HONO mixing ratio differences and coupling regimes

The investigation of the coupling regimes of the forest to the air layer above the canopy, as well as the coupling inside the forest is crucial to study the surface-atmosphere  
 25 exchange of trace gases. The shaded and more humid subcanopy featured different environmental conditions than the atmosphere above the canopy, where the humidity

21123

was lower and photochemistry was more active. Vertical mixing processes link these two environments. As an indicator for the effectiveness of vertical mixing, the detection of coherent structures was used. These provide effective mixing and can be used to infer the coupling between the subcanopy, canopy and the layer above canopy. Thomas  
 5 and Foken (2007) defined five different coupling regimes:

*Wave motion (Wa)*. The flow above the canopy is dominated by linear wave motion rather than by turbulence, and therefore decoupled from the subcanopy and the canopy.

*Decoupled canopy (Dc)*. The air above the canopy is decoupled from the canopy, because there is no transfer of energy and matter into and out of the canopy by coherent  
 10 structures.

*Decoupled subcanopy (Ds)*. The layer above the canopy is coupled to the canopy, but decoupled from the subcanopy.

*Coupled sub canopy by sweeps (Cs)*. The coherent exchange between the canopy air and the subcanopy is forced by strong sweep motion of coherent structures only.

*Fully coupled canopy (C)*. The layer above the canopy, the canopy and the sub  
 15 canopy are in a fully coupled state.

The diel cycle of HONO mixing ratio differences (above canopy minus below canopy) shown in Figs. 5 and 6 can be subdivided into four typical periods:

1) Early night (17:30–21:00 CET): There was no photolytic sink (sunset at  
 20 17:30 CET), but also no turbulent exchange (Wa). These were from a micrometeorological perspective the most stable conditions during the day, with a complete decoupling of the forest from the layer above the canopy (Wa, Dc). Due to the increasing nighttime values in the dry period, absolute HONO differences increased as well and induce a higher variability at nighttime (Fig. 5). Mixing ratio  
 25 differences of up to  $-170 \text{ ppt}$  were measured. The higher HONO mixing ratios close to the forest floor in the early night can be explained by formation of HONO at the ground surface and accumulation in the trunk space, since the exchange with the layer above the canopy was very limited due to the decoupling of the forest. Above the canopy, mixing ratios increased at a lower rate or were fairly

21124

constant during this period, resulting in negative mixing ratio differences. The increasing differences could be observed similarly in the RH (Fig. 5), which was not affected by photolysis or chemical reactions. The sign of the difference changed during the early night at about 21:00 CET, when mixing ratios above canopy rose quickly and exceeded the values measured near the ground. This effect was more pronounced at the end of the dry period, when nighttime maximum values were much higher than during the first two days after the rain event.

- 2) Late night to early morning (21:00–06:30 CET): Increasing mixing ratios above the canopy, exceeding the values below the canopy caused positive mixing ratio differences (max. ~240 ppt). The higher mixing ratios above the canopy from the late night to the early morning were either caused by advection of HONO-enriched air masses above the forest canopy (which was the case for high mixing ratios on 23 September) or potentially by wetting of the canopy and release of adsorbed HONO according to the mechanism described by Trick (2004).
- 3) Early morning to noon (06:30–13:00 CET): HONO mixing ratios decreased at both heights due to photolysis. The mixing ratio differences were close to zero (within the uncertainty of both instruments, see Sect. 3.1), although photolytic lifetimes differ by a factor of 10–25 (median values) between both heights (Fig. 6). Around noon of clear-sky days, lifetimes were about 10 min above and 100–250 min below the canopy. If no exchange between both heights had occurred, a steep mixing ratio gradient should be observed. However, coupling of all forest compartments to the layer above the canopy was achieved during this period, as indicated by the dominance of C and Cs regimes with Ds intermissions (Fig. 5). Hence, effective mixing has offset the differences in HONO lifetimes due to photolysis (Fig. 6).
- 4) Afternoon (13:00–17:30 CET): When decoupling of the subcanopy (Ds) became the predominant regime in the early afternoon (13:00) and HONO lifetime ratios increased to a factor of 25–40 (median values), we always measured negative

21125

mixing ratio differences with a surprisingly low variation over the entire dry period (Figs. 5 and 6).

The HONO/NO<sub>x</sub> vertical differences (not shown) have a similar diel cycle (see Figs. 5 and 6), as variations were mainly caused by the HONO mixing ratios (see Sect. 3.2). Differences were in the range of –6% (evening) to +5% (at night) and around zero from early morning to noon (very similar to HONO itself). Therefore, changes in the HONO mixing ratio differences can be attributed to changes in source or sink processes leading to higher (or lower) values in relation to NO<sub>x</sub> values. Under conditions with virtually no turbulent exchange of the forest with the layer above canopy (Dc and Wa regimes), which occurred in the late afternoon/early night we found systematically higher values below canopy. This is a strong indication that HONO was formed and/or released at the ground.

The diel cycle of the mixing ratio differences can be explained by differences in source and sink processes throughout the canopy, whereas the magnitude of these mixing ratio differences is determined by the exchange conditions as derived from the coherent structures.

### 3.4 Case study: 23 September

In order to exemplify the interplay of different HONO source and sink processes, Fig. 7 shows a contour plot of RH and the HONO mixing ratios measured at 0.5 and 24.5 m above the ground on 23 September.

From midnight to 06:30 CET, HONO mixing ratios were typically higher above the canopy than below. The HONO/NO<sub>x</sub> ratios were between 6 and 10% at both heights. We found a positive correlation ( $r^2=0.78$ ) with RH at 24.5 m but no correlation at the lower height ( $r^2=0.07$ ) during the same time period. This might be attributed to higher RHs up to 90% at the ground, representing a transition to a completely wetted vegetation surface (i.e. formation of epicuticular water films) above 90% RH (Burkhardt and Eiden, 1994; Klemm et al., 1998; Lammel, 1999) thus leading to HONO uptake.

21126

During the first two hours after sunrise (06:30–08:30 CET), HONO mixing ratios decreased continuously with a rate of  $60 \text{ ppt h}^{-1}$  above the canopy and with  $40 \text{ ppt h}^{-1}$  close to the forest floor. If only photolysis was active, the calculated loss rate (i.e.,  $j(\text{HONO}) \times [\text{HONO}]$ ) above the canopy would be faster ( $76 \text{ ppt h}^{-1}$ ) than observed. Below the canopy, the calculated loss rate would be much slower ( $5.5 \text{ ppt h}^{-1}$ ) due to shading. This discrepancy can be explained by vertical mixing. Downward mixing of HONO-depleted air from aloft resulted in a much faster loss rate below the canopy than calculated from photolysis alone. The overall HONO loss is expected to be faster than the photolytic loss alone since the mixed layer growth in the morning contributes to a decrease of near surface HONO that was trapped in the thermodynamically stable NBL.

From 08:30 CET until noontime, slightly decreasing HONO mixing ratios ( $10\text{--}15 \text{ ppt h}^{-1}$  most likely due to photolysis and mixing) were accompanied by a fast decrease of RH by  $6\% \text{ h}^{-1}$  due to surface heating, causing rising surface temperatures. Therefore both measured variables were well correlated, but the correlation was mainly driven by radiation. Even though HONO lifetimes above and below canopy differ by a factor of 10 to 25 (median values) in the morning (Fig. 6), the difference in HONO mixing ratios is less than 5 ppt from 10:00–12:00 CET, which is within the uncertainty of both instruments. This can be explained by vertical exchange, taking place within the HONO lifetime above canopy.

Just after noontime, we observed a pronounced increase of HONO mixing ratios and of HONO/NO<sub>x</sub> ratios at both heights, with a simultaneous increase of RH by 10%. These patterns were most likely caused by passing clouds, increasing the HONO lifetime by a factor of three (from 9 min to 26 min above canopy, see Fig. 3), but were also related to a change in wind direction.

After the noontime peak, HONO mixing ratios decreased again at both heights but with a lower rate below canopy due to the 10 times lower photolysis frequencies. Further increases of lifetime ratios in the afternoon from 25 to 40 may have contributed to the increasing differences. While these differences were counter-balanced by effective

21127

vertical mixing as indicated by a predominantly full coupling of the forest to the air layer above the canopy (C, Cs) in the morning hours, in the afternoon the HONO mixing ratio differences were maintained due to a lack of vertical mixing in the decoupled subcanopy (Ds) regime. Thus, only during periods when the subcanopy or even the whole forest are decoupled from the layer above the canopy, the different loss and production processes acting close to the forest floor and in the upper canopy become obvious. We propose a combination of lifetime differences due to shading of the canopy and the intensity of vertical mixing to explain the observed mixing ratio differences during daytime.

About two hours before sunset, HONO mixing ratios started to increase at both measurement heights. Above canopy, an increase rate of  $40 \text{ ppt h}^{-1}$  led to a slightly higher level of HONO mixing ratios of  $70 \pm 16 \text{ ppt}$ , whereas close to the forest floor, an increase rate of about  $90 \text{ ppt h}^{-1}$  resulted in a higher and nearly constant level of about  $200 \pm 20 \text{ ppt}$ . The steep increase in HONO mixing ratios at the ground coincided with an obvious RH increase below canopy, which is not as pronounced as above canopy.

After sunset, photolysis does no longer affect the atmospheric lifetime of HONO. Thus, the occurrence of different HONO mixing ratios and at the same time different HONO/NO<sub>x</sub> ratios (about 5% higher below canopy) at the two measuring heights provide evidence for different HONO-source processes throughout the canopy. The slight increase above the canopy and the strong increase below canopy in the absence of solar radiation and turbulent exchange with the air layer above canopy (Wa) give a strong indication that HONO was formed and released at the ground. We found a good correlation ( $r^2=0.74$ ) of HONO and RH for the whole period from 16:00–20:30 CET close to the forest floor due to accumulation of HONO and humidity below the canopy after decoupling of the forest. Above the canopy the correlation coefficient is very weak ( $r^2=0.3$ ).

Between 20:30–21:00 CET a steep increase of HONO mixing ratios was observed. This event is considered to be dominated by an air mass change and not by local HONO production or release. Simultaneously, ozone mixing ratios dropped by about

21128



## References

- Alicke, B., Platt, U., and Stutz, J.: Impact of nitrous acid photolysis on the total hydroxyl radical budget during the Limitation of Oxidant Production Pianura/Padana Produzione di Ozono study in Milan, *J. Geophys. Res.*, 107, 8196, doi:10.1029/2000JD000075, 2002.
- 5 Ammann, M., Kalberer, M., Arens, F., Lavanchy, V., Gäggler, H. W., and Baltensperger, U.: Nitrous acid formation on soot particles: surface chemistry and the effect of humidity, *J. Aerosol. Sci.*, 29, 1031–1032, 1998.
- Ammann, M., Rössler, E., Strekowski, R., and George, C.: Nitrogen dioxide multiphase chemistry: uptake kinetics on aqueous solutions containing phenolic compounds, *Phys. Chem. Chem. Phys.*, 7, 2513–2518, 2005.
- 10 Andrés-Hernández, M. D., Notholt, J., Hjorth, J., and Schrems, O.: A DOAS study on the origin of nitrous acid at urban and non-urban sites, *Atmos. Environ.*, 30, 175–180, 1996.
- Arens, F., Gutzwiller, L., Baltensperger, U., Gäggler, H. W., and Ammann, M.: Heterogeneous reaction of NO<sub>2</sub> on diesel soot particles, *Environ. Sci. Technol.*, 35, 2191–2199, 2001.
- 15 Arens, F., Gutzwiller, L., Gäggeler, H. W., and Ammann, M.: The reaction of NO<sub>2</sub> with solid anthracene (1,2,10-trihydroxy-anthracene), *Phys. Chem. Chem. Phys.*, 4, 3684–3690, 2002.
- Aubin, D. G. and Abbatt, J. P. D.: Interaction of NO<sub>2</sub> with hydrocarbon soot: focus on HONO yield, surface modification, and mechanism, *J. Phys. Chem. A*, 111, 6263–6273, 2007.
- Ayers, G. P.: Comment on regression analysis of air quality data, *Atmos. Environ.*, 35, 2423–2425, 2001.
- 20 Baldocchi, D., Falge, E., Gu, L., Olson, R., Hollinger, D., Running, S., Anthoni, P., Bernhofer, C., Davis, K., Evans, R., Fuentes, J., Goldstein, A., Katul, G., Law, B., Lee, X., Malhi, Y., Meyers, T., Munger, W., Oechel, W., Paw U, K. T., Pilegaard, K., Schmid, H. P., Valentini, R., Verma, S., Vesala, T., Wilson, K., and Wofsy, S.: FLUXNET: a new tool to study the temporal and spatial variability of ecosystem-scale carbon dioxide, water vapor, and energy flux densities, *B. Am. Meteorol. Soc.*, 82, 2415–2434, 2001.
- Bejan, I., Aal, Y. A. E., Barnes, I., Benter, T., Bohn, B., Wiesen, P., and Kleffmann, J.: The photolysis of ortho-nitrophenols: a new gas phase source of HONO, *Phys. Chem. Chem. Phys.*, 8, 2028–2035, doi:10.1039/b516590c, 2006.
- 30 Bröske, R., Kleffmann, J., and Wiesen, P.: Heterogeneous conversion of NO<sub>2</sub> on secondary organic aerosol surfaces: A possible source of nitrous acid (HONO) in the atmosphere?, *Atmos. Chem. Phys.*, 3, 469–474, doi:10.5194/acp-3-469-2003, 2003.

21131

- Burkhardt, J. and Eiden, R.: Thin water films on coniferous needles, *Atmos. Environ.*, 28, 2001–2017, 1994.
- Calvert, J. G., Yarwood, G., and Dunker, A. M.: An evaluation of the mechanism of nitrous acid formation in the urban atmosphere, *Res. Chem. Intermediat.*, 20, 463–502, 1994.
- 5 Febo, A., Perrino, C., and Allegrini, I.: Measurement of nitrous acid in Milan, Italy, by DOAS and diffusion denuders, *Atmos. Environ.*, 30, 3599–3609, 1996.
- Finlayson-Pitts, B. J., Wingen, L. M., Sumner, A. L., Syomin, D., and Ramazan, K. A.: The heterogeneous hydrolysis of NO<sub>2</sub> in laboratory systems and in outdoor and indoor atmospheres: an integrated mechanism, *Phys. Chem. Chem. Phys.*, 5, 223–242, 2003.
- 10 Finlayson-Pitts, B. J.: Reactions at surfaces in the atmosphere: integration of experiments and theory as necessary (but not necessarily sufficient) for predicting the physical chemistry of aerosols, *Phys. Chem. Chem. Phys.*, 11, 7760–7779, 2009.
- Foken, T.: *Micrometeorology*, Springer, Berlin-Heidelberg, 308 pp., 2008.
- Foken, T., Meixner, F. X., Falge, E., Zetzsch, C., Serafimovich, A., Bargsten, A., Behrendt, T., Biermann, T., Breuninger, C., Gerken, T., Hunner, M., Lehmann-Pape, L., Hens, K., Jocher, G., Kesselmeier, J., Lüers, J., Mayer, J.-C., Moravek, A., Plake, D., Riederer, M., Rütz, F., Scheibe, M., Schier, S., Siebicke, L., Sörgel, M., Staudt, K., Trebs, I., Tsokankunku, A., Welling, M., Wolf, V., and Zhu, Z.: *Atmospheric transport and chemistry in forest ecosystems-overview of the EGER-project, in preparation*, 2010.
- 20 Frankenberger, E.: Untersuchungen über den Vertikalaustausch in den unteren Dekametern der Atmosphäre, *Ann. Meteorol.*, 4, 358–374, 1951.
- George, C., Strekowski, R. S., Kleffmann, J., Stemmler, K., and Ammann, M.: Photoenhanced uptake of gaseous NO<sub>2</sub> on solid organic compounds: a photochemical source of HONO?, *Faraday Discuss.*, 130, 195–210, 2005.
- 25 Gerstberger, P., Foken, T., and Kalbitz, K.: The Lehstenbach and Steinkreuz catchments in NE Bavaria, in: *Biogeochemistry of Forested Catchments in a Changing Environment: a German Case Study*, edited by: Matzner, E., Ecological Studies, Springer Verlag, Heidelberg, 15–44, 2004.
- Gower, S. T., Kucharik, C. J., and Norman, J. M.: Direct and indirect estimation of leaf area index,  $f_{\text{APAR}}$ , and net primary production of terrestrial ecosystems, *Remote Sens. Environ.*, 70, 29–51, 1999.
- 30 Gustafsson, R. J., Orlov, A., Griffiths, P. T., Cox, R. A., and Lambert, R. M.: Reduction of NO<sub>2</sub> to nitrous acid on illuminated titanium dioxide aerosol surfaces: implications for photocatalysis

21132

- and atmospheric chemistry, *Chem. Commun.*, 37, 3936–3938, 2006.
- Gustafsson, R. J., Kyriakou, G., and Lambert, R. M.: The molecular mechanism of tropospheric nitrous acid production on mineral dust surfaces, *Chem. Phys. Chem.*, 9, 1390–1393, 2008.
- Gutzwiller, L., Arens, F., Baltensberger, U., Gäggler, H. W., and Ammann, M.: Significance of semivolatile diesel exhaust organics for secondary HONO formation, *Environ. Sci. Technol.*, 36, 677–682, 2002a.
- Gutzwiller, L., George, C., Rössler, E., and Ammann, M.: Reaction kinetics of NO<sub>2</sub> with resorcinol and 2,7-naphthalenediol in the aqueous phase at different pH, *J. Phys. Chem. A*, 106, 12045–12050, 2002b.
- Hanst, P. L., Spence, J. W., and Miller, M.: Atmospheric chemistry of n-nitroso dimethylamine, *Environ. Sci. Technol.*, 11, 403–405, 1977.
- Harrison, R. M. and Kitto, A.-M. N.: Evidence for a surface source of atmospheric nitrous acid, *Atmos. Environ.*, 28, 1089–1094, 1994.
- He, Y., Zhou, X., Hou, J., Gao, H., and Bertman, S. B.: Importance of dew in controlling the air-surface exchange of HONO in rural forested environments, *Geophys. Res. Lett.*, 33, L02813, doi:10.1029/2005GL024348, 2006.
- Heland, J., Kleffmann, J., Kurtenbach, R., and Wiesen, P.: A new instrument to measure gaseous nitrous acid (HONO) in the atmosphere, *Environ. Sci. Technol.*, 35, 3207–3212, 2001.
- Jenkin, M. E., Cox, R. A., and Williams, D. J.: Laboratory studies of the kinetics of formation of nitrous acid from the thermal reaction of nitrogen dioxide and water vapour, *Atmos. Environ.*, 22, 487–498, 1988.
- Killus, J. P. and Whitten, G. Z.: Background reactivity in smog chambers, *Int. J. Chem. Kinet.*, 22, 547–575, 1990.
- Kleffmann, J., Becker, K. H., and Wiesen, P.: Heterogeneous NO<sub>2</sub> conversion processes on acid surfaces: possible atmospheric implications, *Atmos. Environ.*, 32, 2721–2729, 1998.
- Kleffmann, J., Becker, K. H., Lackhoff, M., and Wiesen, P.: Heterogeneous conversion of NO<sub>2</sub> on carbonaceous surfaces, *Phys. Chem. Chem. Phys.*, 1, 5443–5450, 1999.
- Kleffmann, J., Heland, J., Kurtenbach, R., Lörzer, J., and Wiesen, P.: A new instrument (LOPAP) for the detection of nitrous acid (HONO), *Environ. Sci. Pollut. R.*, 4, 48–54, 2002.
- Kleffmann, J., Kurtenbach, R., Lörzer, J., Wiesen, P., Kalthoff, N., Vogel, B., and Vogel, H.: Measured and simulated vertical profiles of nitrous acid – Part I: Field measurements, *Atmos. Environ.*, 37, 2949–2955, 2003.

21133

- Kleffmann, J., Benter, T., and Wiesen, P.: Heterogeneous reaction of nitric acid with nitric oxide on glass surfaces under simulated atmospheric conditions, *J. Phys. Chem. A*, 108, 5793–5799, 2004.
- Kleffmann, J., Gavrioloaiei, T., Hofzumahaus, A., Holland, F., Koppmann, R., Rupp, L., Schlosser, E., Siese, M., and Wahner, A.: Daytime formation of nitrous acid: a major source of OH radicals in a forest, *Geophys. Res. Lett.*, 32, L05818, doi:10.1029/2005GL022524, 2005.
- Kleffmann, J.: Manual LOPAP-3, version 1.3.0, Bergische Universität Wuppertal, QUMA Elektronik and Analytik GmbH, Wuppertal, 2006.
- Kleffmann, J., Lörzer, J. C., Wiesen, P., Kern, C., Trick, S., Volkamer, R., Rodenas, M., and Wirtz, K.: Intercomparison of the DOAS and LOPAP techniques for the detection of nitrous acid (HONO), *Atmos. Environ.*, 40, 3640–3652, 2006.
- Kleffmann, J.: Daytime sources of nitrous acid (HONO) in the atmospheric boundary layer, *Chem. Phys. Chem.*, 8, 1137–1144, 2007.
- Klemm, O., Burkhardt, J., and Gerchau, J.: Leaf wetness: A quantifiable parameter in deposition studies, in: *Proceedings of the EUROTRAC-2 Symposium 98: Transport and chemical transformation in the troposphere*, edited by: Borell, P. M and Borell, P., WITpress, Southampton, 238–242, 1999.
- Kraus, A. and Hofzumahaus, A.: Field measurements of atmospheric photolysis frequencies for O<sub>3</sub>, NO<sub>2</sub>, HCHO, CH<sub>3</sub>CHO, H<sub>2</sub>O<sub>2</sub>, and HONO by UV spectroradiometry, *J. Atmos. Chem.*, 31, 161–180, 1998.
- Lammel, G. and Perner, D.: The atmospheric aerosol as a source of nitrous acid in the polluted atmosphere, *J. Aerosol. Sci.*, 19, 1199–1202, 1988.
- Lammel, G. and Cape, J. N.: Nitrous acid and nitrite in the atmosphere, *Chem. Soc. Rev.*, 25, 361–369, 1996.
- Lammel, G.: *Formation of Nitrous Acid: Parameterisation and Comparison with Observations*, Max Planck Institute for Meteorology, Hamburg, report No. 286, 36, 1999.
- Legendre, P. and Legendre, L.: *Numerical Ecology*, 2nd English ed., Developments in Environmental Modelling, Elsevier Science BV, Amsterdam, 1998.
- Monge, M. E., D'Anna, B., Mazri, L., Giroir-Fendler, A., Ammann, M., Donaldson, D. J., and George, C.: Light changes the atmospheric reactivity of soot, *P. Natl. Acad. Sci. USA*, 107, 6605–6609, 2010.
- Moravek, A.: Vertical distribution of reactive and non-reactive trace gases in and above a spruce

21134

- canopy, master thesis, University Karlsruhe, Germany, 124 pp., 2008
- Ndour, M., D'Anna, B., George, C., Ka, O., Balkanski, Y., Kleffmann, J., Stemmler, K., and Ammann, M.: Photoenhanced uptake of NO<sub>2</sub> on mineral dust: laboratory experiments and model simulations, *Geophys. Res. Lett.*, 35, L05812, doi:10.1029/2007GL032006, 2008.
- 5 Notholt, J., Hjorth, J., and Raes, F.: Formation of HNO<sub>2</sub> on aerosol surfaces during foggy periods in the presence of NO and NO<sub>2</sub>, *Atmos. Environ.*, 26, 211–217, 1992.
- Oren, R., Schulze, E.-D., Matyssek, R., and Zimmermann, R.: Estimating photosynthetic rate and annual carbon gain in conifers from specific leaf weight and leaf biomass, *Oecologia*, 70, 187–193, 1986.
- 10 Perner, D. and Platt, U.: Detection of nitrous acid in the atmosphere by differential optical absorption, *Geophys. Res. Lett.*, 6, 917–920, 1979.
- Pitts Jr., J. N., Biermann, H. W., Winer, A. M., and Tuazon, E. C.: Spectroscopic identification and measurement of gaseous nitrous acid in dilute auto exhaust, *Atmos. Environ.*, 18, 847–854, 1984.
- 15 Pitts Jr., J. N., Grosjean, D., Cauwenberghe, K. V., Schmid, J. P., and Fitz, D. R.: Photooxidation of aliphatic amines under simulated atmospheric conditions: formation of nitrosamines, nitramines, amides, and photochemical oxidant, *Environ. Sci. Technol.*, 12, 946–953, 1978.
- Qin, M., Xie, P., Su, H., Gu, J., Peng, F., Li, S., Zeng, L., Liu, J., Liu, W., and Zhang, Y.: An observational study of the HONO–NO<sub>2</sub> coupling at an urban site in Guangzhou City, South China, *Atmos. Environ.*, 43, 5731–5742, 2009.
- 20 Reisinger, A. R.: Observations of HNO<sub>2</sub> in the polluted winter atmosphere: possible heterogeneous production on aerosols, *Atmos. Environ.*, 34, 3865–3874, 2000.
- Rohrer, F., Bohn, B., Brauers, T., Brüning, D., Johnen, F.-J., Wahner, A., and Kleffmann, J.: Characterisation of the photolytic HONO-source in the atmosphere simulation chamber SAPHIR, *Atmos. Chem. Phys.*, 5, 2189–2201, doi:10.5194/acp-5-2189-2005, 2005.
- 25 Rubio, M. A., Lissi, E., and Villena, G.: Nitrite in rain and dew in Santiago City, Chile. Its possible impact on the early morning start of the photochemical smog, *Atmos. Environ.*, 36, 293–297, 2002.
- Rubio, M. A., Lissi, E., and Villena, G.: Factors determining the concentration of nitrite in dew from Santiago, Chile, *Atmos. Environ.*, 42, 7651–7656, 2008.
- 30 Sakamaki, F., Hatakeyama, S., and Akimoto, H.: Formation of nitrous acid and nitric oxide in the heterogeneous dark reaction of nitrogen dioxide and water vapour, *Int. J. Chem. Kinet.*, 15, 1013–1029, 1983.

21135

- Saliba, N. A., Yang, H., and Finlayson-Pitts, B. J.: Reaction of gaseous nitric oxide with nitric acid on silica surfaces in the presence of water at room temperature, *J. Phys. Chem. A*, 105, 10339–10346, 2001.
- Serafimovich, A., Thomas, C., and Foken, T.: Vertical and horizontal transport of energy and matter by coherent motions in a tall spruce canopy, *Bound.-Lay. Meteorol.*, submitted, 2010.
- 5 Sjödin, Å.: Studies of the diurnal variation of nitrous acid in urban air, *Environ. Sci. Technol.*, 22, 1086–1089, 1988.
- Sleiman, M., Gundel, L. A., Pankow, J. F., Jacob, P., Singer, B. C., and Destailats, H.: Formation of carcinogens indoors by surface-mediated reactions of nicotine with nitrous acid, leading to potential thirdhand smoke hazards, *P. Natl. Acad. Sci. USA*, 107, 6576–6581, 2010.
- 10 Sokal, R. R. and Rohlf, F. J.: *Biometry – The Principles and Practice of Statistics in Biological Research*, 3rd ed., W. H. Freeman, New York, 1995.
- Sonntag, D.: Important new values of the physical constants of 1986, vapor pressure formulations based on the ITS-90 and psychrometer formulae, *Z. Meteorol.*, 70, 340–344, 1990.
- 15 Staudt, K. and Foken, T.: Documentation of reference data for the experimental areas of the Bayreuth Centre for Ecology and Environmental Research (BayCEER) at the Waldstein site, University of Bayreuth, Dept. of Micrometeorology Bayreuth, report No. 37, 2007.
- Staudt, K., Falge, E., Pyles, R. D., Paw U, K. T., and Foken, T.: Sensitivity and predictive uncertainty of the ACASA model at a spruce forest site, *Biogeosciences Discuss.*, 7, 4223–4271, doi:10.5194/bgd-7-4223-2010, 2010.
- 20 Stemmler, K., Ammann, M., Donders, C., Kleffmann, J., and George, C.: Photosensitized reduction of nitrogen dioxide on humic acid as a source of nitrous acid, *Nature*, 440, 195–198, 2006.
- Stemmler, K., Ndour, M., Elshorbany, Y., Kleffmann, J., D'Anna, B., George, C., Bohn, B., and Ammann, M.: Light induced conversion of nitrogen dioxide into nitrous acid on submicron humic acid aerosol, *Atmos. Chem. Phys.*, 7, 4237–4248, doi:10.5194/acp-7-4237-2007, 2007.
- 25 Stull, R. B.: *An Introduction to Boundary Layer Meteorology*, Atmospheric and Oceanographic Sciences Library, Kluwer Academic Publishers, Dordrecht, 670 pp., 1988.
- Stutz, J., Alicke, B., and Neftel, A.: Nitrous acid formation in the urban atmosphere: gradient measurements of NO<sub>2</sub> and HONO over grass in Milan, Italy, *J. Geophys. Res.*, 107(D22), 8192, doi:10.1029/2001JD000390, 2002.
- 30 Stutz, J., Alicke, B., Ackermann, R., Geyer, A., Wang, S., White, A. B., Williams, E. J., Spicer, C. W., and Fast, J. D.: Relative humidity dependence of HONO chemistry in urban

21136

- areas, *J. Geophys. Res.*, 109, D03307, doi:10.1029/2003JD004135, 2004.
- Su, H., Cheng, Y. F., Cheng, P., Zhang, Y. H., Dong, S., Zeng, L. M., Wang, X., Slanina, J., Shao, M., and Wiedensohler, A.: Observation of nighttime nitrous acid (HONO) formation at a non-urban site during PRIDE-PRD2004 in China, *Atmos. Environ.*, 42, 6219–6232, 2008.
- 5 Svensson, R., Ljungström, E., and Lindqvist, O.: Kinetics of the reaction between nitrogen dioxide and water vapour, *Atmos. Environ.*, 21, 1529–1539, 1987.
- Thomas, C. and Foken, T.: Detection of long-term coherent exchange over spruce forest using wavelet analysis, *Theor. Appl. Climatol.*, 80, 91–104, 2005.
- Thomas, C. and Foken, T.: Flux contribution of coherent structures and its implications for the exchange of energy and matter in a tall spruce canopy, *Bound.-Lay. Meteorol.*, 123, 317–337, doi:10.1007/s10546-006-9144-7, 2007.
- 10 Trebs, I., Bohn, B., Ammann, C., Rummel, U., Blumthaler, M., Königstedt, R., Meixner, F. X., Fan, S., and Andreae, M. O.: Relationship between the NO<sub>2</sub> photolysis frequency and the solar global irradiance, *Atmos. Meas. Tech.*, 2, 725–739, doi:10.5194/amt-2-725-2009, 2009.
- 15 Trick, S.: Formation of nitrous acid on urban surfaces - a physical-chemical perspective-, Ph.D. thesis, University Heidelberg, Germany, 290 pp., 2004.
- Veitel, H.: Vertical profiles of NO<sub>2</sub> and HONO in the boundary layer, Ph.D. thesis, University Heidelberg, Germany, 270 pp., 2002.
- Vogel, B., Vogel, H., Kleffmann, J., and Kurtenbach, R.: Measured and simulated vertical profiles of nitrous acid – Part II. Model simulations and indications for a photolytic source, *Atmos. Environ.*, 37, 2957–2966, 2003.
- 20 Wainmann, T., Weschler, C. J., Lioy, P. J., and Zhang, J.: Effects of surface type and relative humidity on the production and concentration of nitrous acid in a model indoor environment, *Environ. Sci. Technol.*, 35, 2200–2206, 2001.
- 25 Wolff, V., Trebs, I., Foken, T., and Meixner, F. X.: Exchange of reactive nitrogen compounds: concentrations and fluxes of total ammonium and total nitrate above a spruce canopy, *Biogeosciences*, 7, 1729–1744, doi:10.5194/bg-7-1729-2010, 2010.
- Yu, Y., Galle, B., Panday, A., Hodson, E., Prinn, R., and Wang, S.: Observations of high rates of NO<sub>2</sub>–HONO conversion in the nocturnal atmospheric boundary layer in Kathmandu, Nepal, *Atmos. Chem. Phys.*, 9, 6401–6415, doi:10.5194/acp-9-6401-2009, 2009.
- 30 Zhang, N., Zhou, X., Shepson, P. B., Gao, H., Alaghmand, M., and Stirn, B.: Aircraft measurement of HONO vertical profiles over a forested region, *Geophys. Res. Lett.*, 36, L15820, doi:10.1029/2009GL038999, 2009.

21137

- Zhou, X., Civerolo, K., Dai, H., Huang, G., Schwab, J., and Demerjian, K.: Summertime nitrous acid chemistry in the atmospheric boundary layer at a rural site in New York State, *J. Geophys. Res.*, 107(D21), 4590, doi:10.1029/2001JD001539, 2002a.
- Zhou, X., He, Y., Huang, G., Thornberry, T. D., Carroll, M. A., and Bertman, S. B.: Photochemical production of nitrous acid on glass sample manifold surface, *Geophys. Res. Lett.*, 29(14), 1681, doi:10.1029/2002GL015080, 2002b.
- 5 Zhou, X., Gao, H., He, Y., Huang, G., Bertman, S. B., Civerolo, K., and Schwab, J.: Nitric acid photolysis on surfaces in low-NO<sub>x</sub> environments: significant atmospheric implications, *Geophys. Res. Lett.*, 30(23), 2217, doi:10.1029/2003GL018620, 2003.

21138

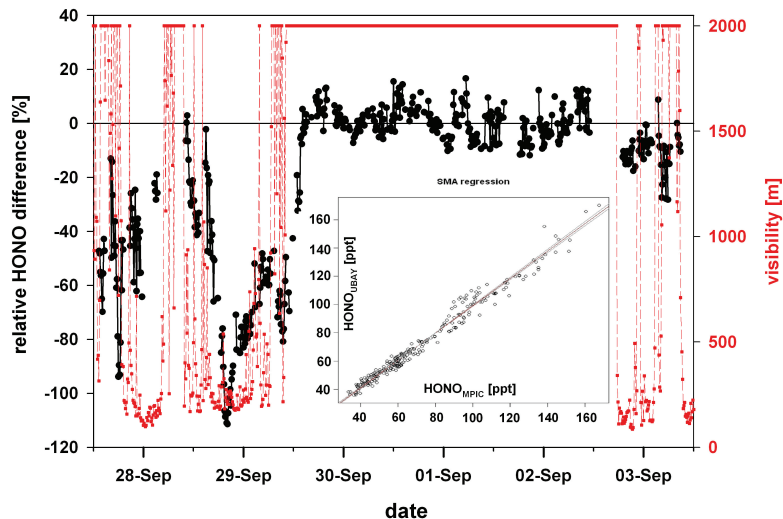


**Fig. 1.** Side-by-side measurements of the two LOPAP instruments from 27 September (noon) to 3 October 2007 (noon) at the “Weidenbrunnen” research site. Relative differences of the HONO signals (black dots) and visibility range (red squares, dashed lines, maximum range 2000 m). The insert shows the regression obtained during dry conditions ( $N=247$ ) from 29 September (14:00 CET) to 2 October (10:00 CET) using standard major axis (SMA) regression. Missing values are due to zero air measurements and calibration of the LOPAP instruments.

21139

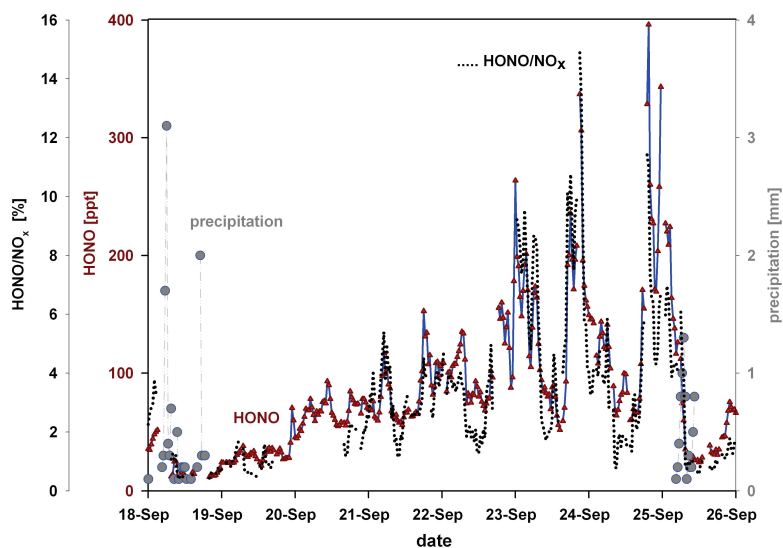


**Fig. 2.** Time series of HONO at 0.5 m above the forest floor (triangles and blue line) and HONO/NO<sub>x</sub> ratio (black dotted line) from 18 (00:00 CET) to 26 (00:00 CET) September 2007 at the “Weidenbrunnen” research site. This dry period was delimited by rain events marked with grey circles (half hourly values).

21140

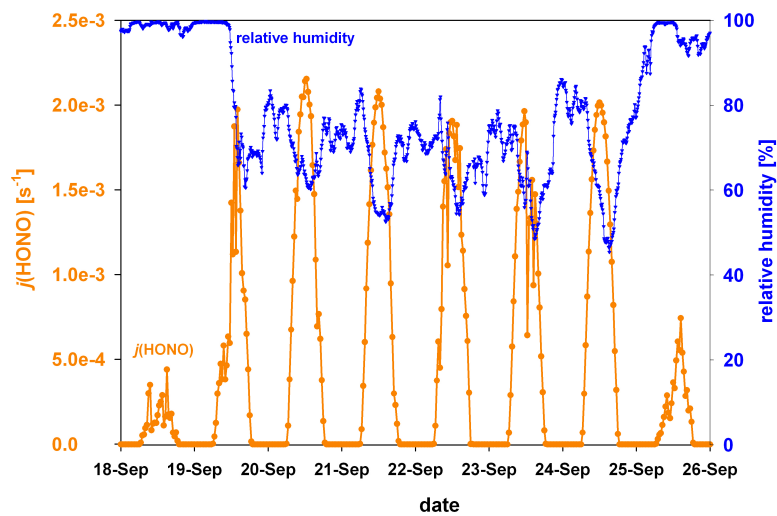


**Fig. 3.** Time series of the HONO photolysis frequency  $j(\text{HONO})$  parameterized from the measured  $\text{NO}_2$  photolysis frequency at a height of 28 m (orange line and dots) and relative humidity measured at the canopy top (21 m) from 18 (00:00 CET) to 26 (00:00 CET) September 2007 at the “Weidenbrunnen” research site.

21141

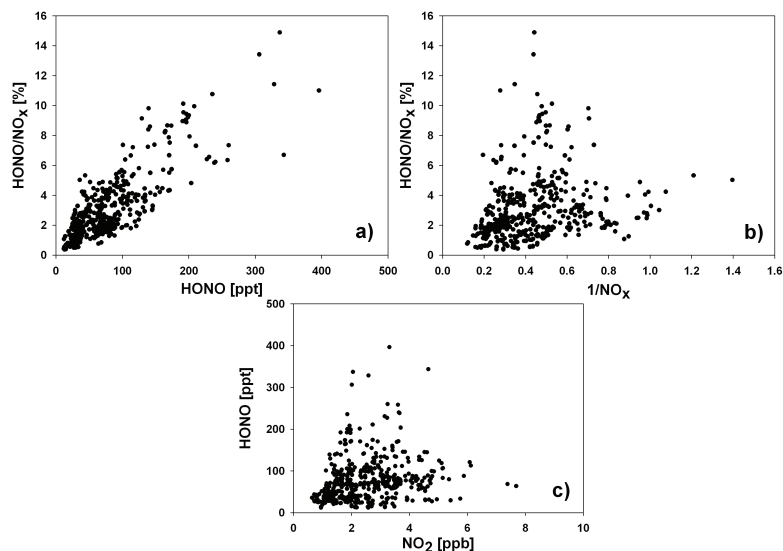


**Fig. 4.** Relationships of HONO and  $\text{NO}_x$  for the measurement height close to the forest floor (0.5 m) for the period 13–25 September at the “Weidenbrunnen” research site. The upper graphs (a) and (b) show a better correlation of  $\text{HONO}/\text{NO}_x$  to HONO than to  $1/\text{NO}_x$ , i.e. variations in  $\text{HONO}/\text{NO}_x$  are more likely explained by variations in HONO mixing ratios than by  $\text{NO}_x$  values. The lower graph shows that HONO and its precursor  $\text{NO}_2$  are not well correlated during the period from 13–25 September.

21142

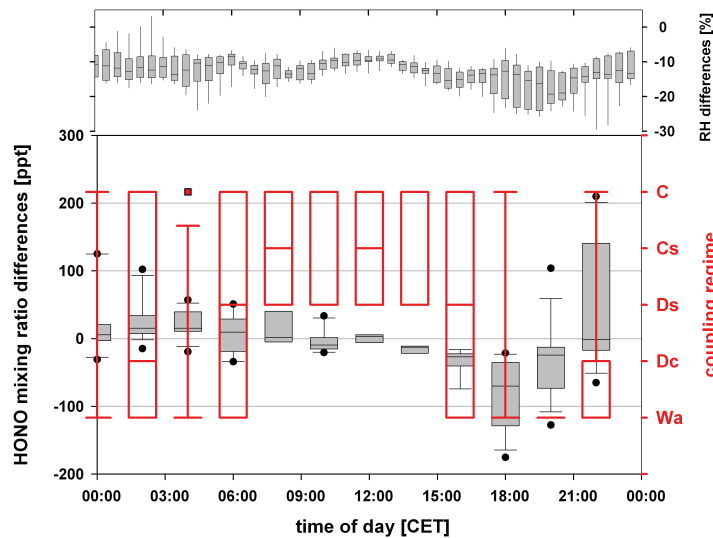


**Fig. 5.** Box-and-whisker plot for coupling regimes (red open bars) and HONO mixing ratio differences (grey filled bars) for the five-day dry period 20–25 September 2007 at the “Weidenbrunnen” research site. The upper panel shows the RH difference between 21 m and the forest floor for comparison (without outliers). The upper end of the boxes represents the 75th percentile, the lower end the 25th percentile and the line within the boxes the median. Whiskers denote the last values within the 10th (lower whisker) and 90th (upper whisker) percentiles. Outliers are marked as points (HONO difference) or squares (coupling regimes). If only whiskers appear, there are no other values between the values marked by the whiskers. From 08:00–14:00 CET there are only C and Ds values but with odd (08:00 CET and 12:00 CET) and even (10:00 CET and 14:00 CET) data points. The median therefore falls in line with the end of the box (“odd-case”) or into the middle (“even-case”).

21143

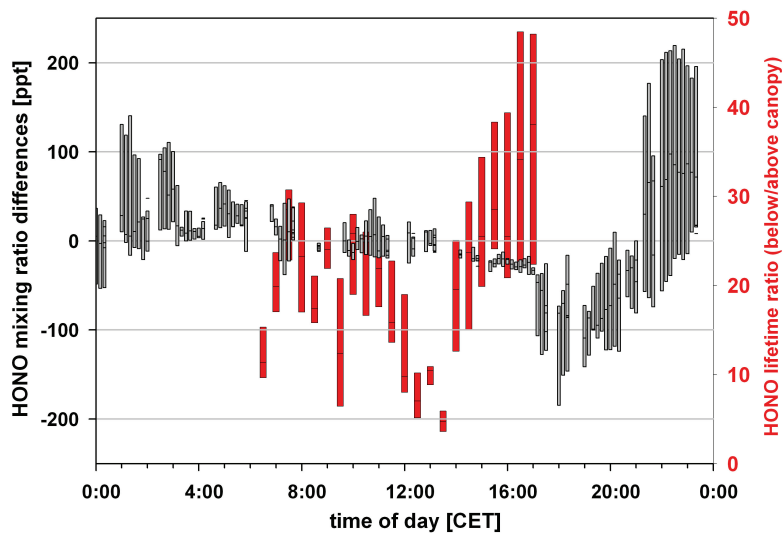


**Fig. 6.** HONO mixing ratio differences (grey bars, 10 min averages) and lifetime ratios (below to above canopy) (red bars, 30 min averages) for the five-day dry period 20–25 September 2007 at the “Weidenbrunnen” research site. The upper end of the boxes represents the 75th percentile, the lower end the 25th percentile and the line within the boxes the median.

21144

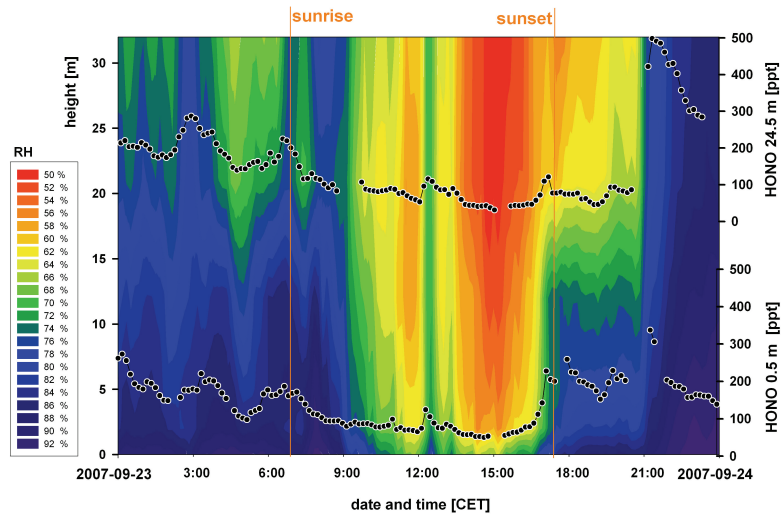


**Fig. 7.** Simultaneous HONO time series at 0.5 m (lower graph, circles and lines) and 24.5 m (upper graph, circles and lines), overlaid with a contour plot of the vertical profile of measured RH (colour-coded 50–92%) for 23 September 2007 at the “Weidenbrunnen” research site. Missing values in the HONO measurements are due to zero air measurements. Sunrise and sunset (inferred from  $j(\text{NO}_2)$  as a proxy for  $j(\text{HONO})$  and global radiation measurements) are marked as vertical (orange) lines.